Counting Rates Modeling for PET Scanners With GATE

David Guez, Frédéric Bataille, Claude Comtat, *Member, IEEE*, Pierre-Francois Honoré, Sébastien Jan, and Sophie Kerhoas

Abstract—Several developments were made in the GATE simulation platform to allow accurate modeling of the count rate performances of PET scanners over a wide range of activity concentrations. A background noise module, a dead time and limited bandwidth modeling for the coincidences, and a delayed coincidence builder were added in the code. The results obtained for the modeling of the ECAT HRRT and Focus 220 scanners with the newly developed modules are discussed. They show that GATE can be used to accurately simulate the single event, prompt coincidence and delayed coincidence rates, from very low activity levels in the field of view up to levels that saturate the acquisition system. The new developments were committed into the public release of GATE, making them available for the whole community, thanks to the open source license under which GATE is published (LGPL).

Index Terms—Bandwidth, dead time, GATE, Geant4, memory buffer, Monte Carlo simulation, positron emission tomography.

I. INTRODUCTION

IN PARALLEL TO the developments of PET scanners, the need for a versatile and accurate simulation code to reproduce the scanner response over a large range of source activity, becomes more and more stringent. For high count rates, the amount of events that are lost due to the detector and the system dead time is not negligible. In addition, the ratio of random to true coincidences and the rate of multiple coincidences increase substantially. These high count rate related phenomena, by decreasing the rate of true coincidences, have a significant impact on the image quality [1]. In order to predict the performances of PET prototypes or to study optimal imaging protocols, the use of accurate and efficient simulation tools is essential, especially in the areas described above [2], [3].

Data loss models for PET systems usually involve several dead time and bandwidth-limited components [4], [5]. They are applied at the detector, coincidence processing, and data transfer and storage levels. They estimate the count loss as a function of the input count rate. The total event rate to be processed by the acquisition system is the sum of the prompt events and the delayed events given by the delayed coincidence window (if it is implemented on the scanner). Consequently, prompt and delayed coincidences have to be included in the modeling of the system count loss. Reilhac *et al.* [3] showed for the block detector ECAT EXACT HR+ scanner that the implementation in the PET-SORTEO simulator of the data loss four-component model of Moisan *et al.* [5] allows to reproduce the count rate performance of the scanner for both prompt and random coincidences over a large range of activities. The GATE [6] simulation toolkit for PET and SPECT systems incorporates natively the time course in the simulation code. This feature allows the explicit simulation of coincidences, based on a temporal coincidence window. This construction incorporates intrinsically random and multiple coincidences in addition to true coincidences; there is no need to simulate them separately. Similarly, data loss modeling components can be explicitly simulated. On the arrival of an event, the next events are discarded during a dead time period according to a paralyzing or non-paralyzing model [7]. L. Simon *et al.* [8] have shown that this event-by-event simulation of dead time was able to reproduce accurately count loss due to a paralyzing or non-paralyzing dead time.

Improvement in the accuracy of the simulated count rate in PET scanners with GATE was known to be possible. Before the GATE version 2.1.0, the processing of the delayed coincidences or the modeling of dead time at the coincidences level had to be performed post-simulation [8]. This work is dedicated to the development of the appropriate GATE classes required for an accurate simulation of the count rate performances of PET systems over a wide range of activities. These classes have been included in GATE version 2.1.0. The modeling of the quantitative response of two block detector PET scanners is presented: the microPET Focus 220 small animal scanner [9] and the ECAT HRRT brain scanner [10].

II. MATERIALS AND METHODS

A. GATE—Overview

GATE is a Geant4 based application [11] intended to be a generic tool for PET and SPECT simulations. Within GATE, Geant4 is used for the generation and the tracking of the particles emitted by the radionuclide, and for the description of the materials. Beyond this, GATE adds the acquisition and signal processing stage, which is an important feature for the complete simulation of PET systems. This component is defined as a list of elementary processors, generically called *event processors*. They represent the block detector readout modeling, energy resolution degradation modeling, energy threshold, dead time mod-

eling, or efficiency loss modeling, among others. The *event processors* structure allows to describe, with a reasonably good accuracy, the data processing chain from the detector readout to the writing of the event on disk.

B. Software Developments

Several features were missing before GATE version 2.1.0 to achieve accurate simulations of coincidence count rate for PET scanners. For this purpose, several improvements were introduced into the code:

1) Background Noise Simulation: In order to reproduce the data acquisition rate at very low activities in the scanner field-of-view (below a few MBq), the events induced by the background noise can not be ignored. The background noise can be due to the electronics or have a physical origin like the natural radioactivity of the crystals. For the Focus and the HRRT scanners, the main source of noise is the natural radioactivity of the Lutetium presents in the LSO crystals.

A new *event processors* was created in such a way that it can be used for the modeling of the electronic noise, as well as any other physical noise. In order to be as generic as possible, the mean time interval between two noise events and their energy distribution are described in a script file. The crystal associated to a noise event is randomly chosen, assuming an equipartition of random rate between all crystals. The background noise events, once inserted, are treated by the GATE's *event processors* like any other detected photons.

2) Coincidence Builder: GATE generates coincidences by opening a coincidence time window for the first single event detected, looking for other single events (referred as coincident events) occurring within this window. This method constrains the second single event to not open its own window, that is, can not participate to more than one coincidence. This model will be referred to as the *single window coincidence mode*. While this method was found to be suitable to reproduce the Focus 220 count rate for prompt and delayed coincidences, it was not the case for the HRRT delayed coincidence count rate. A new coincidence builder model was implemented in GATE, where each single event opens its own coincidence window, and can therefore be part of two different coincidences. This new model will be referred to as the *multiple window coincidence mode*.

To illustrate this effect, let's consider the following example for a coincidence window of 3 ns and three single events: the first at time zero, the second after 2 ns and the third after 4 ns. With the *single window coincidence mode*, only one coincidence with events one and two is generated. With the *multiple window coincidence mode*, two coincidences are generated: one with events one and two, and one with events two and three. The *multiple window coincidence mode* was found to be suitable to reproduce the HRRT count rates for prompt and delayed coincidences.

3) Multiple Coincidences: For high source activities, the rate of multiple coincidences can not be neglected. Before version 2.1.0, GATE rejected all multiple coincidence events. Since the modeled scanners actually do not reject them, a new option was implemented in the code to allow recording multiple coincidences.

4) Delayed Coincidence Window: The random coincidences are intrinsically accounted for in GATE. In practice, the random coincidence rate is usually experimentally estimated by a delayed coincidence window. Before version 2.1.0, GATE did not provide such delayed coincidences. The simulated random coincidence rate was usually estimated by using the event identification marker, provided by GATE, but obviously not experimentally accessible.

Because delayed coincidences participate in most PET systems to the global coincidence dead time, the code was upgraded so that separated coincidence lines can be defined, with their own delay (which is equal to zero for prompt coincidences). At the required level, these separate coincidence lines can be multiplexed into an unique line. An other reason for simulating delayed coincidences is to mimic the statistical properties of the net true coincidences: prompt minus delayed coincidences are not Poisson distributed.

5) Coincidence Event Processors: One of the most interesting feature of GATE is its ability to describe and simulate the acquisition and signal processing stages with *event processors*. So far, these *event processors* applied only to the single events (*single event processors*). Since coincidence builders are also electronic modules, it should be possible to use the same modeling for coincidence processing. The following *coincidence event processors* have been defined.

- Paralysable or non-paralysable dead times. These *coincidence event processors* applied to prompt or delayed coincidences separately, or to both if merged. Several dead time *event processors* can be inserted sequentially, but there are no dedicated *event processors* for a dead time that combines both paralyzable and non paralyzable components.
- Memory buffers. This module mimics the effect of limited transfer rate and is characterized by two parameters: the reading frequency ν and the memory depth D. Data are filling the memory buffer, which is then emptied out at a fixed clock reading frequency ν. This reading frequency ν defines the upper output rate limit. When the buffer size limit D is reached, any new event is discarded until a new reading clock tick occurs. A non-null buffer depth D allows to face a temporary input data flow rise.

C. Experimental Setup

1) HRRT and Focus Scanners: The microPET Focus 220 is a scanner dedicated to small animal imaging such as rodents (mice and rats) and primates (macaque or small baboon). It consists of 168 LSO blocks organized in 4 rings. Each detector block is composed of a matrix of 12×12 crystals with dimensions of $1.5 \times 1.5 \times 10 \text{ mm}^3$ each.

The HRRT is a brain positron tomograph made of 8 detector heads arranged in an octagon. Each head consists of 9×13 detector blocks of 8×8 dual-layer $2.1 \times 2.1 \times (10 + 10) \text{ mm}^3$ LSO-LYSO crystals. The head-to-head distance is 469 mm and the axial field-of-view is 253.5 mm. The phoswitch configuration allows the scanner to measure depth of interaction, preserving a good spatial resolution toward the edge of the transverse field-of-view.

For both scanners, the width of the coincidence time window was set to $2\tau = 6$ ns, and multiple coincidences were accepted by the data acquisition system.

For the HRRT, the outputs of the detector blocks are processed by analog boards that assign the arrival time of the detected events with a 2 ns binning resolution, identify the crystal of interaction, performs energy qualification (the energy of valid single events is within a defined energy window), and form digital single event words. At the level of the detector head, the single event words of energy qualified events are multiplexed by the "Detector Head Interface" (DHI) board. Each DHI board can tranfer up to four single event words to the coincidence controller (CC) during each master clock cycle (256 ns). In the CC, each detector head is placed in coincidence with all other detector heads except for the two adjacent heads and itself, giving 20 module pairs that are processed by 20 data processing field-programmable gate arrays (FPGAs). During a master clock cycle, the digitized time values of single events are compared, and if they occurred during the same coincidence timing window 2τ of 6 ns, the event is encoded into a 64-bit list mode coincidence event word. In a second coincidence chain, delayed events are determined by the delayed coincidence time window method. The coincidence event words (prompt and delayed coincidences) are transfered to the acquisition computer through an optical fiber. Up to four 64-bit coincidence event words can be sent every 256 ns (1 Gbit/s). The 64-bit coincidence event words are stored directly on the hard disk of the acquisition computer.

For the modeling of both scanners with GATE, the phantoms containing the radioactive sources and the crystals were included in the material description. For the HRRT, a tungsten shielding against radioactivity outside the field of view was also modeled. For both scanners, a global energy resolution of 26% at 511 keV was modeled for each block detector. The GATE modeling has been previously validated in term of spatial resolution and scattered coincidence fraction for the Focus [12] and for the HRRT [13].

2) Experiments: In order to validate the new *event processors* against experimental data, a cylindrical phantom was placed in the field of view of each scanner, and uniformly filled with a radioactive solution. The count rates were then measured for different activity levels in the cylinder, except for one experiment. The same configuration was then simulated with GATE. For each scanner, two different classes of experiment were performed: one to adjust the parameters of the *event processors*, and another to test the robustness of the *event processors* parameters by using a modified experimental setup.

For the HRRT, two phantoms were used: a mouse-like consisting of a 6.6 cm long and 1.35 cm radius cylinder (37.8 ml), and a 20 cm diameter and 20 cm long cylinder. For the Focus 220, only the former was used. In the following sections, five experiments will be referred to as followed:

— experiment H1: *event processors* parameters adjustment for the HRRT with the mouse phantom and an energy window of [350, 750] keV;

— experiment H2: *event processors* parameters robustness for the HRRT with the 20 cm cylinder and an energy window of [400, 650] keV;

— experiment H3: *event processors* parameters robustness for the HRRT with the 20 cm cylinder and a lower level discriminator (LLD) between 200 and 400 keV (the source activity in the cylinder was kept constant);

— experiment F1: *event processors* parameters adjustment for the Focus 220 with the mouse phantom and an energy window of [350, 750] keV;

— experiment F2: *event processors* parameters robustness for the Focus 220 with the mouse phantom and an energy window of [250, 750] keV.

The single event count rates, as well as the prompt and delayed coincidence count rates, were recorded and compared to the simulation results.

3) Data Analysis and Model Adjustment: The three following experimental count rates were measured:

— the energy qualified single event count rate per detector block, summed over all blocks;

— the prompt and delayed coincidence count rates measured at the coincidence-processing circuity level (referred to as *head curves*);

— the prompt and delayed coincidences count rates once they are written to disk in listmode format and rebinned to sinograms (referred to as *histogrammed curves*).

For both scanners, based on the H1 or F1 experiments, the following procedure was used to adjust the *event processors* parameters in our simulation needed to reproduce the experimental single event rate:

a) the experimental single event count rate curve in the very low activity region is fitted with a straight line (this is were contribution from dead time is negligible);

b) the fitted line is extrapolated to zero activity to find the background noise level;

c) the fitted line is extrapolated to the high activity region and compared to the measured data to estimate the dead time; this is a model-dependant procedure and is performed on a block-to-block basis;

d) following these two steps, the simulated single event rates are compared to the experimental data. The corresponding ratio is calculated and examined to ensure that it is approximately constant over the whole activity range for both scanners. It is also used to deduce a global efficiency for each single event detection, before dead time modeling. The resulting simulation to experiment ratio is approximately equal to 1 for all activities. This efficiency takes into account the quantum efficiency of the crystal, as well as the light transfer between crystals and photomultiplier. Generally, for a given scanner, the global efficiency parameter is fitted once and is assumed not to change with different experiments as long as the set-up of the scanner is not drifting. If the gain of the scanner is known to evolve with time (which is the case for the HRRT scanner [14]), this parameter has to be re-adjusted.

Once the experimental single event count rates are reproduced, the parameters for the coincidence count rates are estimated. For the Focus 220 and the HRRT, the prompt plus delayed coincidences count rate curve is characterized by two regions. Below a certain activity level A_t, whose value depends on the source geometry, the count rate increases monotonically
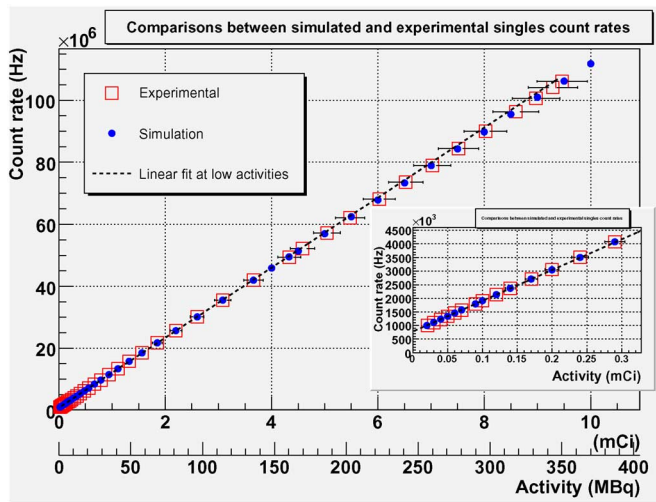
Fig. 1. Global single event count rate comparison between experimental and simulation results for the H1 experiment. In the lower right corner, the same data are plotted for the lowest activities only. The activity in the phantom was measured with a 5% uncertainty.

with the source activity. Above this activity level, the count rate is flat and has reached the memory buffer reading frequency. The value of the memory buffer depth is set such as to reproduce the shape of the prompt plus delayed coincidences count rate curve around A_t, in the transition zone between both regions. By comparing the simulated and the measured prompt plus delayed coincidences rates for activity levels below A_t, the coincidence builder dead time is estimated.

III. RESULTS

Samples were taken from the active cylinders and activity concentration measured in a gamma counter. The uncertainty of the gamma counter calibration is 3% and the variability on the samples measurments is 4%. The activity concentration of the cylinders is therefore known with a precision of 5%.

A. Modeling of the ECAT HRRT Scanner

1) Experiment H1: The linear fit of the experimental single event count rate in the very low activity region, once extrapolated to zero activity, gives a global background noise level of 772.8 kHz modeled as a Poisson distribution in GATE. This fit is then used to estimate the dead time at high activities. As a result, a non paralysable dead time of 109 ns/block is used for the single events. It should be noted that the dead time is modeled before energy qualification, and therefore its value differs from values measured with experimental energy qualified single event rates.

A global efficiency of 93.75% is used in the simulation in order to fit the experimental output. With these parameters, the simulated single event count rate is very close to the experimental one, even for low activities (Fig. 1).

The prompt and delayed coincidence count rates, as measured at the coincidence-processing circuity level, are well reproduced with the *multiple window coincidence mode*, a non paralysable dead time of 20 ns and a buffer reading frequency of 14.45 MHz.
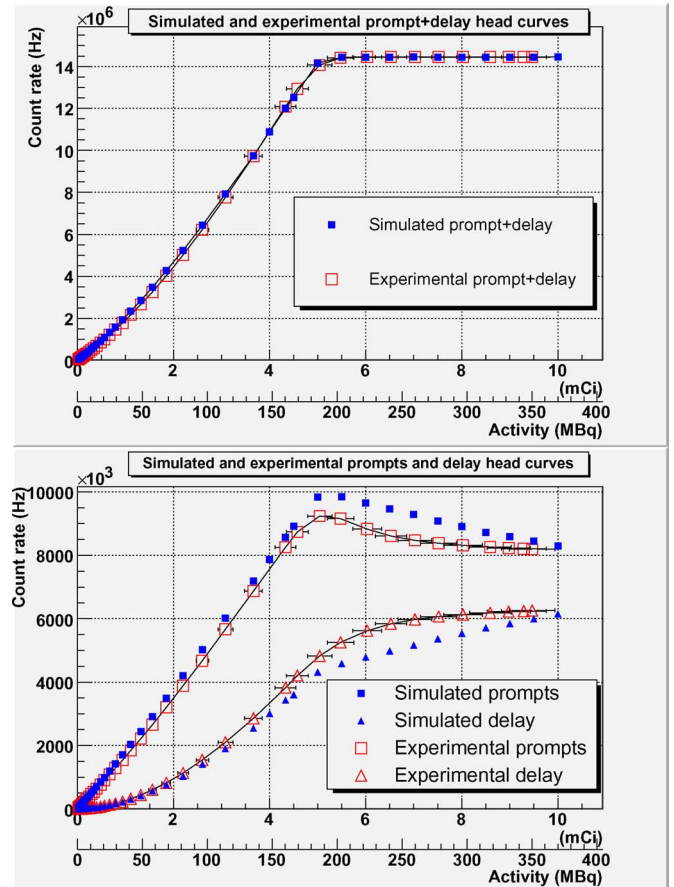

Fig. 2. Comparison between simulated and measured coincidence count rates from the *head curves* of the H1 experiment. The upper panel shows the sum of the prompt and delayed coincidence count rates, whereas the lower panel shows the individual rates. The activity in the phantom was measured with a 5% uncertainty.

These results are shown on Fig. 2. The upper limit on the coincidence rate corresponding to the buffer reading frequency is clearly visible on the sum of the prompt and delayed coincidences. This buffer corresponds to the data transportation via the optical fibers between the coincidence-processing circuity and the acquisition computer.

All the GATE modeling parameters of the *event processors* for the HRRT are summarized in Table I and in Fig. 3. The comparison between the simulation and experimental results is summarized in Table II. The systematic difference observed in the prompt and delayed coincidence count rates at high activities (above 5 mCi, when the coincidence processor saturates) leads to a huge relative difference in the corrected prompt minus delayed coincidence (net trues, including both scattered and unscattered coincidences) count rates. For this reason, the comparison is also given for 0 to 4 mCi typical range as used in practice. Note that the maximum relative difference for the prompt, delayed, and net true coincidences does not necessary occurs at the same activity level.

2) Experiment H2: To test the robustness of the simulation model, data from another experimental setup were simulated. The same parameters as for experiment H1 were used. However, as the H2 experiment was acquired one year after H1, the efficiency had to be changed from 93.75% to 88.03%. This change

Parameter	value
single event processors	
Background noise level	772.8 kHz
Efficiency	93.75 %
Dead time model	non paralysable
Dead time	109 ns per block
Coincidences builder	
Coincidence window	*multiple window coincidence mode*
Keep multiples	yes
coincidence event processors	
Dead time model	non paralysable
Dead time	20 ns
Buffer reading frequency	14.45 MHz
Buffer depth	64 Coincidences

Fig. 4. Global single event count rate comparison between experimental and simulation for the H2 experiment. In the lower right corner, the same data are plotted for the lowest activities only, showing the good agreement obtained within this useful activities range. Statistical errors bars are plotted for both experiment and simulation points. The activity in the phantom was measured with a 5% uncertainty.
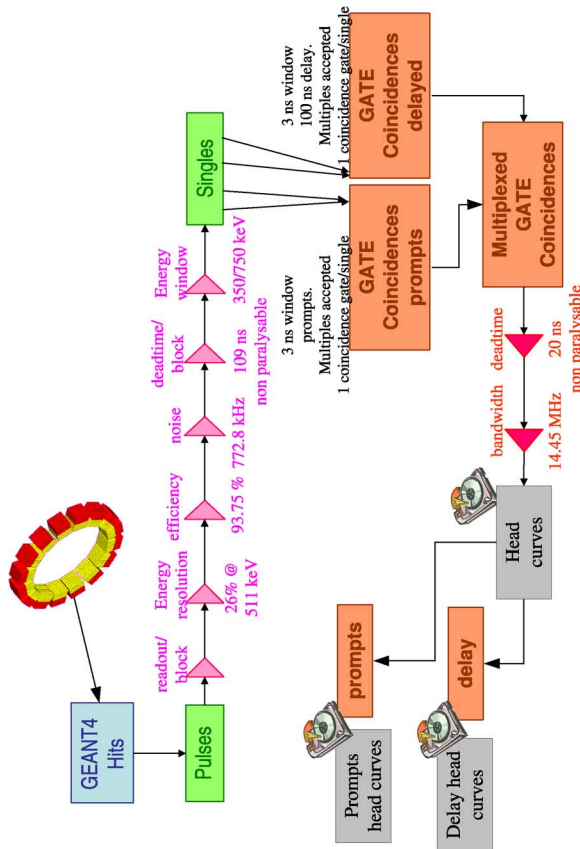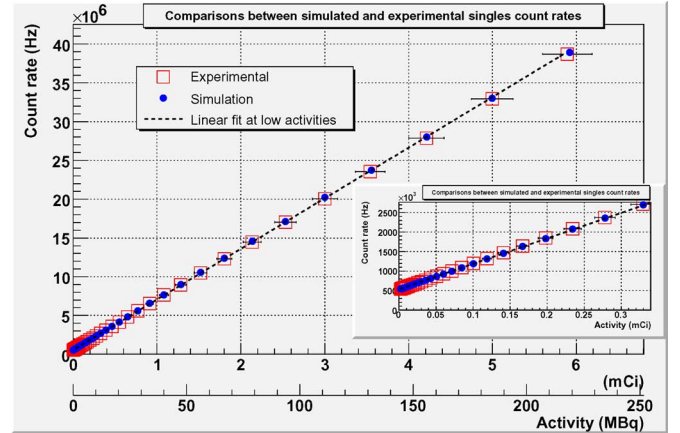

Fig. 3. Scheme of the acquisition model of the ECAT HRRT scanner.

TABLE II
SUMMARY OF THE HRRT SIMULATION RESULTS FOR EXPERIMENT H1. MAXIMUM RELATIVE DIFFERENCE $(simulation - experimental)$ $/experimental$ IS REPORTED FOR THE SPECIFIED ACTIVITY RANGE

	0-10 mCi	0-4 mCi
Head curves		
Prompts	10.67 %	10.67 %
Delayeds	14.62 %	10.84 %
Prompts - delayeds (net trues)	64.83 %	15.68 %

is likely due to the experimental systematic shift of the photomultiplier gain, and is compatible with the gain changes reported in [14]. Whereas the global efficiency between experiments H1 and H2 had to be decreased by 6.1%, the single event rate measured during the daily quality control of the scanner, normalized to the phantom activity, decreased by 4.7% between the days of both experiments.

The comparison of the simulated and experimental count rates, shown in Fig. 4 and Fig. 5 exhibits a good agreement. The quantitative comparison of experimental and simulation results are summarized in Table III. Note that the level at which the coincidence processor saturates (14.45×10^6 prompt plus delayed coincidences per second) was not reached with the H2 experiment.

3) H3 Experiment: For this experiment, the single event count rates were measured for different LLDs values and compared with the simulation results. The cylinder source consisted of Germanium 68, and the source activity was considered as constant during the measurements. The modeling parameters listed in Table I remained unchanged. Table IV summarized the discrepancies of the absolute single event rate between experiment and simulation.

B. Modeling of the Focus 220 Scanner

1) F1 Experiment: The linear fit of the observed single event count rate at very low activity, once extrapolated to zero activity, gives a global background noise level of 132.1 kHz again modeled as a Poisson distributed background noise in GATE. When the fit is extrapolated at high activities, the block-by-block count losses are well modeled with a non paralysable dead time of 110.4 ns. These parameters, along with an efficiency of 91%, are sufficient to reproduce the experimental single event count rate for all activities (as shown in Fig. 6).

The *single window coincidence mode* is used for the coincidence builder. A non paralysable dead time of 37.4 ns allows to reproduce the coincidence count rate measured at the coincidence-processing circuity level. The comparison is shown in Fig. 7.

Once the coincidences are written on disk, the count rates are well modeled with a buffer having an event per event readout frequency of 3.45 MHz (equal to the experimental output limit flow). The simulation results are in good agreement with the
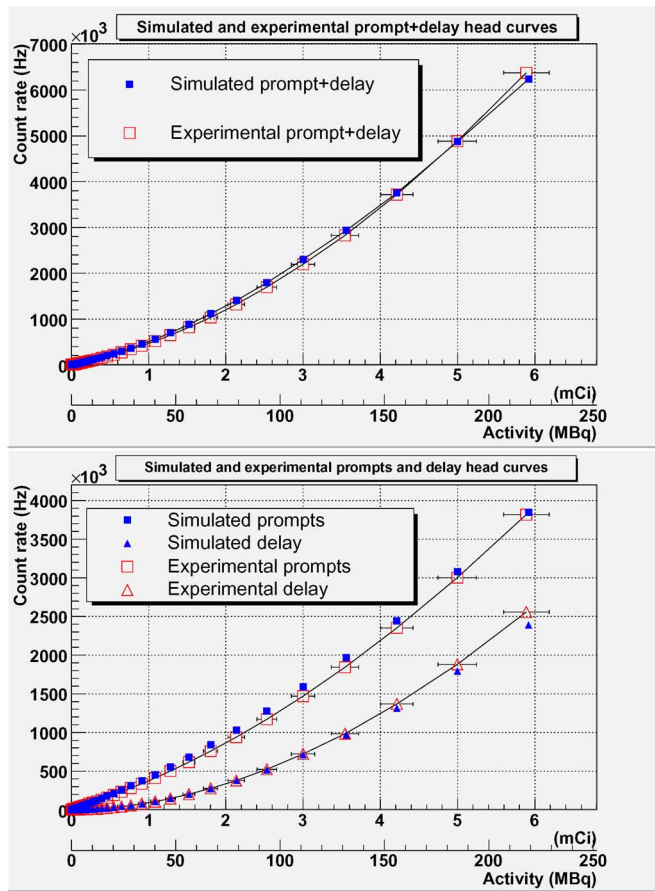
Fig. 5. Comparison between simulated and measured coincidence count rates from the *head curves* for the H2 experiment. The upper panel shows the sum of the prompt and delayed coincidence count rates, whereas the lower panel shows the individual rates. The activity in the phantom was measured with a 5% uncertainty.
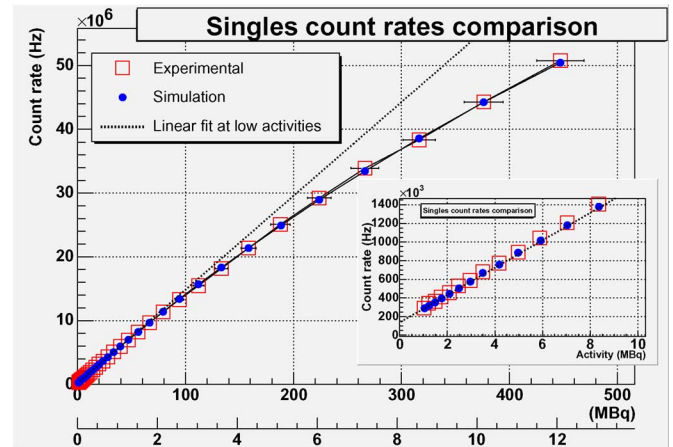

Fig. 6. Comparison of global single event count rates for simulation and experimental data of the F1 experiment. In the lower right corner, the same data are plotted for the lowest activities only. The activity in the phantom was measured with a 5% uncertainty.

TABLE III
SUMMARY OF THE HRRT SIMULATION RESULTS FOR EXPERIMENT H2.
MAXIMUM RELATIVE DIFFERENCE $(simulation - experimental)/experimental$ IS REPORTED FOR THE WHOLE ACTIVITY RANGE

	0-6 mCi
Head curves	
Prompts	10.9 %
Delayeds	8.9 %
Prompts - delayeds (net trues)	17.7 %

TABLE IV
EXPERIMENT H3: RELATIVE DIFFERENCE BETWEEN THE SIMULATED AND THE
MEASURED GLOBAL SINGLE EVENT COUNT RATE AS A FUNCTION OF THE
LLD VALUE

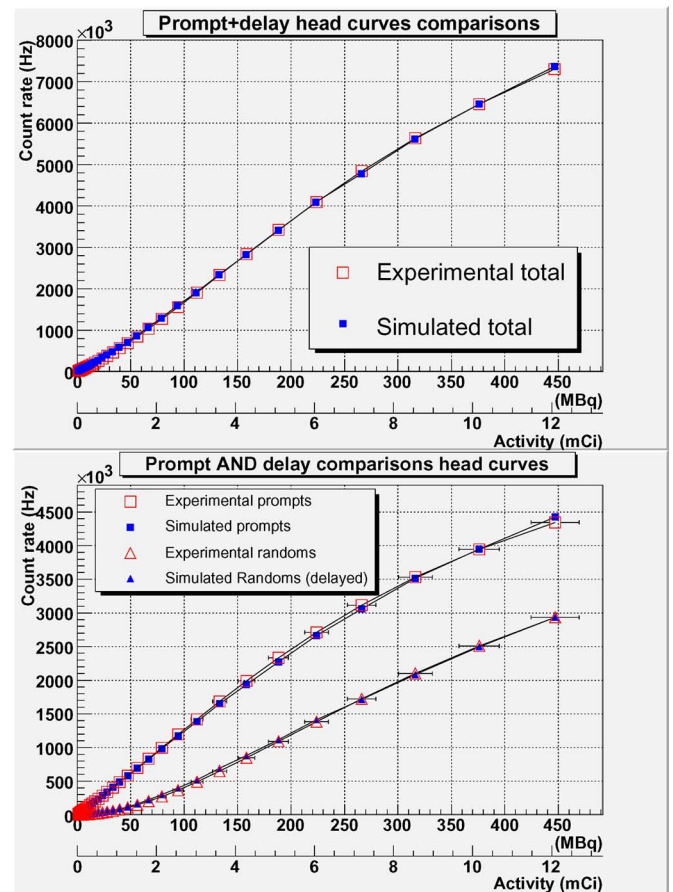| Energy window	Count rate difference
200-650 [keV]	21.7 %
250-650 [keV]	5.4 %
300-650 [keV]	1.0 %
350-650 [keV]	2.1 %
400-650 [keV]	5.6 %

Fig. 7. Comparison of simulated and experimental coincidences count rates from the *head curves* for the F1 experiment. The upper panel shows the sum of the prompt and delayed coincidence count rates, whereas the lower panel shows the individual rates. The activity in the phantom was measured with a 5% uncertainty.

experimental data, for the prompt and delayed coincidences, individually, and for their sum (Fig. 8).

All the *event processors* modeling parameters for the Focus 220 are summarized in Table V and in Fig. 9. The comparison

between the simulated and experimental results is summarized in Table VI. Because systematic differences are observed at low activities for the delayed coincidences, the results for activities above 1 mCi are also given. Moreover, because of systematic
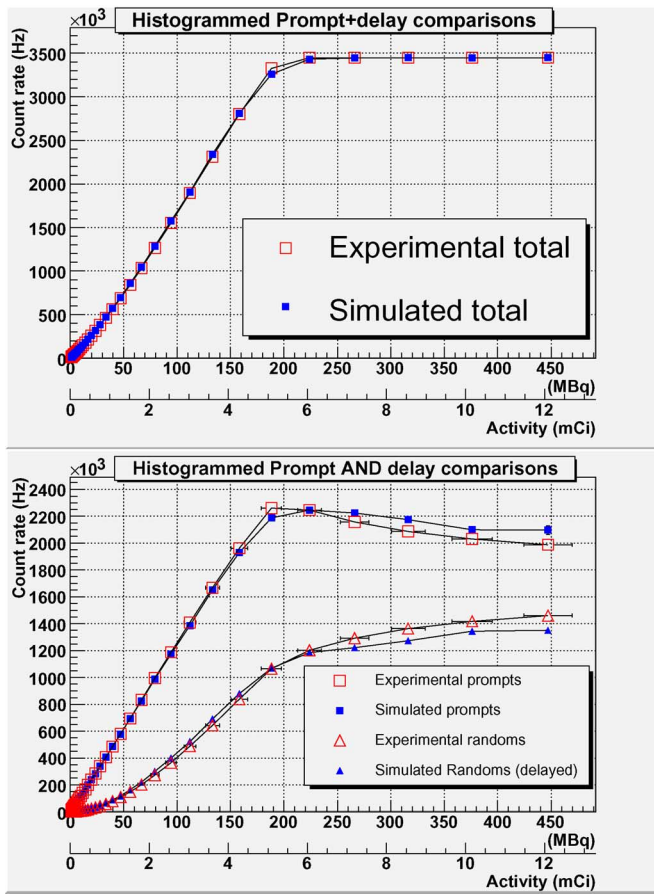
Fig. 8. Comparison of simulated and experimental coincidence count rates from the *histogrammed curves* for the F1 experiment. The upper panel shows the sum of the prompt and delayed coincidence count rates, whereas the lower panel shows the individual rates. The activity in the phantom was measured with a 5% uncertainty.

Fig. 9. Scheme of the acquisition model of the Focus 220 scanner.

TABLE V
SUMMARY OF THE FOCUS 220 *event processors* MODELING PARAMETERS

Parameter	value
single event processors	
Background noise level	132.1 kHz
Efficiency	91.0 %
Dead time model	non paralysable
Dead time	110.4 ns
Coincidences builder	
Coincidence window	*single window coincidence mode*
Keep multiples	yes
coincidence event processors	
Dead time model	non paralysable
Dead time	37.4 ns
Buffer reading frequency	3.45 MHz
Buffer depth	8 Coincidences

TABLE VI
SUMMARY OF THE FOCUS 220 SIMULATION RESULTS FOR F1 EXPERIMENT.
MAXIMUM RELATIVE DIFFERENCE $(simulation - experimental)/$
$experimental$ IS REPORTED FOR THE SPECIFIED ACTIVITY RANGE

	0-12 mCi	1-12 mCi	1-5 mCi
Head curves			
Prompts	5 %	2.8 %	2.8 %
Delayeds	37.8 %	12.9 %	12.9 %
Prompts - delayeds (net trues)	8.15%	8.15 %	8.15 %
Histogrammed curves			
Prompts	5.5 %	5.5 %	1.7 %
Delayeds	38.6 %	13 %	13 %
Prompts - delayeds (net trues)	41.6%	41.6 %	6.7 %

IV. DISCUSSIONS

The *event processors* modules used to model the HRRT and the Focus 220 scanners with GATE allow, over a wide range of activities, to reproduce the experimental single event and coincidence count rates at different levels of the data acquisition processing. One should note that these *event processors* modules are used to describe global count loss effects, and are not intended to account for for each specific detail of the data acquisition electronics. For instance, the background noise module is used to describe the total background noise count rate, no matter where these events are coming from (such as lutetium natural radioactivity and electronic self noise level separation). From Figs. 4 and 6, the background rate has a discernible effect on the single event count rate only below a few MBq in the scanner field-of-view. It contributes to more than 50% of the total single event rate at 1 MBq, for exemple at the end of a 90 minute ^{11}C

differences at high activities, the results are also given for activities between 1 and 5 mCi.

2) F2 Experiment: The single event count rates for the F2 experiment, for which the energy window was changed to 250–750 keV, are shown in Fig. 10. The modeling parameters listed in Table V remained unchanged.
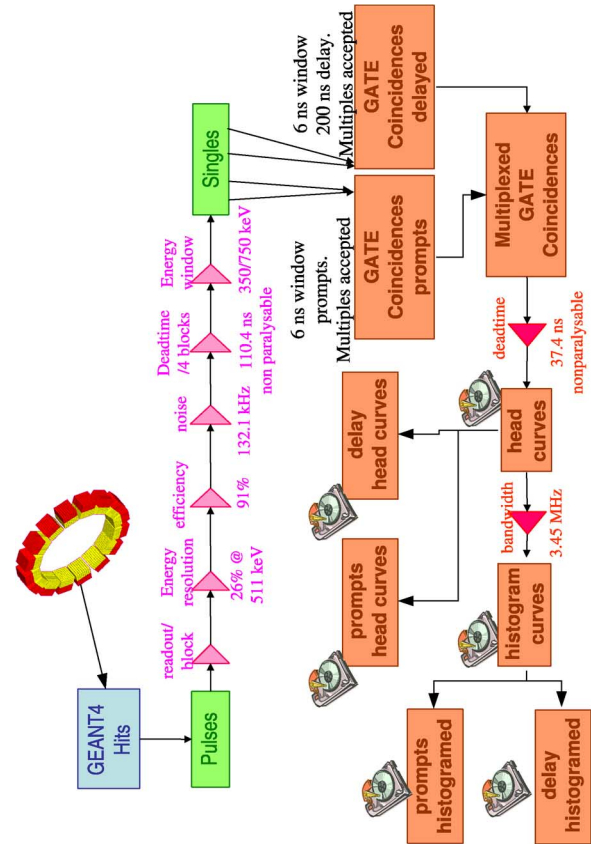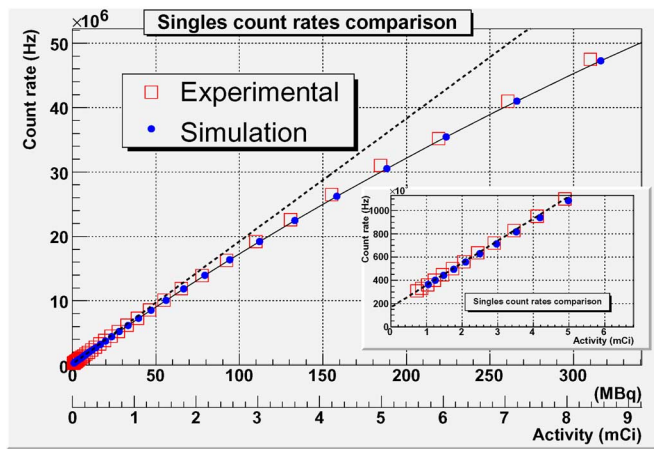
Fig. 10. Comparison of global single event count rates for simulation and experimental data for the F2 experiment. In the lower right corner, the same data are plotted for the lowest activities only. The activity in the phantom was measured with a 5% uncertainty.

study. For most realistic cases, the non simulation of the background will not have a perceivable impact.

The memory buffer modeling involves several parameters not unequivocally determined by the experimental results. Even if the readout frequency is clearly fixed by the coincidence count rate upper limit, a range of buffer depth values can reproduce the experimental data. The main point is that the coincidences count rate losses can be accurately modeled by a memory buffer readout module; the details of the underlying effects are out of the scope of this study.

The global modeling used in our studies is accurate enough to reproduce the count rate performances of both scanners for the simulated experimental setups. The H2 experiment simulation results show that the *event processors* parametrization does not strongly depend on the diameter of the object being imaged. The results of the H3 experiment show a good robustness of the *event processors* parameters for LLD values between 250 and 400 keV. Under 250 keV (200 keV in the case of this experiment), the limits of this model appear.

The results of the F2 experiment simulation show that the count loss parameterization is valid for energy windows down to 250 keV. Although available in GATE, the explicit modeling of pile-up effects was not included in the simulation. Only explicit dead-time at the level of the block detector was modeled for the single events, before applying energy thersholds, and it was found to be accurate enough for the Focus for lower level discriminator values down to 250 keV.

V. CONCLUSION AND PERSPECTIVES

In order to model accurately the single event and the coincidence count rate performances of PET scanner with GATE over a wide range of activities, several new modules were developed. A background noise module was necessary to reproduce the single event count rate at very low activity, in particular

for LSO scanners. As count losses occur not only for the single events, but also for the coincidences, dead-time and memory buffer readout modules were developed specifically for the coincidences. A delayed coincidence builder module was added, as most PET scanners estimate the random coincidence rate with a delayed coincidence window and these delayed coincidences that increases the global dead time of the system.

The modeling of the ECAT HRRT and the Focus 220 scanners with the newly developed modules shows that GATE can be used to accurately simulate the single event, prompt coincidence and delayed coincidence rates, from very low activity levels in the field of view up to levels that saturate the acquisition system.

These news developments represent an important step in performing realistic simulation studies for improving pre-clinical and clinical acquisition protocols.

REFERENCES

[1] C. Lartizien, P. E. Kinahan, and C. Comtat, "A lesion detection observer study comparing 2-dimensional versus fully 3-dimensional whole-body PET imaging protocols," *J. Nucl. Med.*, vol. 45, no. 4, pp. 714–723, 2004.
[2] J. Wear, J. Karp, R. Freifelder, D. Mankoff, and G. Muehllehner, "A model for the high count rate performance of NaI-based PET detectors," *IEEE Trans. Nucl. Sci.*, vol. 45, pp. 1231–1237, Jun. 1998.
[3] A. Reilhac *et al.*, "PET-SORTEO: A Monte Carlo-based simulator with high count rate capabilities," *IEEE Trans. Nucl. Sci.*, vol. 51, pp. 46–52, Feb. 2004.
[4] L. Eriksson, K. Wienhard, and M. Dahlbom, "A simple data loss model for positron camera systems," *IEEE Trans. Nucl. Sci.*, vol. 41, pp. 1566–1570, Aug. 1994.
[5] C. Moisan, J. G. Rogers, and J. L. Douglas, "A count rate model for PET and its application to an LSO HR PLUS scanner," *IEEE Trans. Nucl. Sci.*, vol. 44, pp. 1219–1224, Jun. 1997.
[6] S. Jan *et al.*, "GATE: A simulation toolkit for PET and SPECT," *Phys. Med. Biol.*, vol. 49, pp. 4543–4561, Oct. 2004.
[7] G. F. Knoll, *Radiation Detection and Measurement*. New York: Wiley, Jan. 2000.
[8] L. Simon, D. Strul, G. Santin, M. Krieguer, and C. Morel, "Simulation of time curves in small animal PET using GATE," *Nucl. Instrum. Methods Phys. Res. A*, vol. 527, pp. 190–194, Jul. 2004.
[9] Y.-C. Tai *et al.*, "Performance evaluation of the microPET Focus: A third-generation microPET scanner dedicated to animal imaging," *J Nucl. Med.*, vol. 46, no. 3, pp. 455–463, Mar. 2005.
[10] L. Eriksson *et al.*, "The ECAT HRRT: NEMA NEC evaluation of the HRRT system, the new high-resolution research tomograph," *IEEE Trans. Nucl. Sci.*, vol. 49, pp. 2085–2088, Oct. 2002.
[11] Geant4 Collaboration, "Geant4-a simulation toolkit," *Nucl. Instrum. Methods Phys. Res. A*, vol. 506, pp. 250–303, Jul. 2003.
[12] S. Jan, C. Comtat, R. Trébossen, and A. Syrota, "Monte Carlo simulation of the MicroPET Focus for small animal," in *Proc. SNM 51st Ann. Meeting*, May 2004, vol. 45, no. 5, p. 420P.
[13] F. Bataille, C. Comtat, S. Jan, and R. Trébossen, "Monte Carlo simulation for the ECAT HRRT using GATE," in *IEEE Nuclear Science Sym. Conf. Record*, Oct. 2004, vol. 4, pp. 2570–2574.
[14] V. Sossi *et al.*, "The second generation HRRT—A multi centre scanner performance investigation," in *IEEE Nuclear Science Symp. Conf. Record*, Oct. 2005, vol. 4, pp. 2195–2199.